THE JOURNAL OF BIOLOGICAL CHEMISTRY VOL. 287, NO. 22, pp. 18843–18853, May 25, 2012

Mapping Targetable Sites on Human Telomerase RNA Pseudoknot/Template Domain Using 2′-OMe RNA-interacting Polynucleotide (RIPtide) Microarrays*[S]

Received for publication, October 24, 2011, and in revised form, March 20, 2012 Published, JBC Papers in Press, March 26, 2012, DOI 10.1074/jbc.M111.316596

Lourdes Gude[‡1], Shaunna S. Berkovitch[§], Webster L. Santos[‡2], Peter S. Kutchukian[‡3], Adam R. Pawloski[¶4], Robert Kuimelis[¶], Glenn McGall[¶], and Gregory L. Verdine[‡§‖5]

From the Departments of [‡]Chemistry and Chemical Biology and [§]Molecular and Cellular Biology, Harvard University, Cambridge, Massachusetts 02138, [¶]Affymetrix Inc., Santa Clara, California 95051, and the [‖]Program in Cancer Chemical Biology, Dana-Farber Cancer Institute, Boston, Massachusetts 02115

Background: Identification of targetable regions in folded RNAs remains a challenge.
Results: A novel RIPtide microarray comprising all 2′-*O*-methylated RNAs 4–8 nucleotides in length has been used to discover biologically active antagonists of human telomerase.
Conclusion: RIPtide microarrays can identify nucleic acid-based ligands that bind folded RNA structures.
Significance: RIPtide technology provides the first completely sequence-unbiased screen for targetable sites on folded RNA targets.

Most cellular RNAs engage in intrastrand base-pairing that gives rise to complex three-dimensional folds. This self-pairing presents an impediment toward binding of the RNA by nucleic acid-based ligands. An important step in the discovery of RNA-targeting ligands is therefore to identify those regions in a folded RNA that are accessible toward the nucleic acid-based ligand. Because the folding of RNA targets can involve interactions between nonadjacent regions and employ both Watson-Crick and non-Watson-Crick base-pairing, screening of candidate binder ensembles is typically necessary. Microarray-based screening approaches have shown great promise in this regard and have suggested that achieving complete sequence coverage would be a valuable attribute of a next generation system. Here, we report a custom microarray displaying a library of RNA-interacting polynucleotides comprising all possible 2′-OMe RNA sequences from 4- to 8-nucleotides in length. We demonstrate the utility of this array in identifying RNA-interacting polynucleotides that bind tightly and specifically to the highly conserved, functionally essential template/pseudoknot domain of human telomerase RNA and that inhibit telomerase function *in vitro*.

Although nearly all therapeutic agents developed to date target proteins, it is now widely recognized that only a minority of proteins are capable of being targeted by the two established classes of therapeutic agents, small molecules and biologicals (1). The realization that the majority of proteins are considered intractable toward targeting by established agents has fueled efforts to develop the therapeutic potential of alternative classes of cellular targets, with RNA being the object of most intensive investigation (2, 3). Although examples are known of small molecules that target RNA potently and specifically (3–5), most efforts have taken advantage of the fact that nucleic acids target each other efficiently and selectively through nucleobase-pairing interactions (2). This mode of intermolecular engagement requires that the target sequence be minimally tied up in competing intramolecular base-pairing interactions. Identifying such accessible elements in an RNA target presents a challenge, as the folding landscape of RNA shows remarkable complexity, with a wide variety of noncanonical pairing motifs augmenting canonical Watson-Crick base-pairing (6). Neither the structural nature of these folds nor the energetic cost of gaining access to particular sites is readily predictable. Thus, the discovery of targetable sites is best accomplished through experimental analysis of ensembles of candidate nucleic acid binders.

An important advance in RNA targeting has been the development of nucleic acid microarrays that have enabled multiple candidate ligand sequences to be evaluated in parallel for binding to a particular target sequence. The pioneering work of Southern and co-workers (7–12) in this area employed microarrays of unmodified oligonucleotides, but synthetically modified nucleic acid analogs (13, 14) have also been employed.

* This work was supported, in whole or in part, by National Institutes of Health Grant R01 GM044853 (to G. L. V.), Grant F32 GM067380 from NRSA (to W. L. S.), and Training Grant T32 GM007598 (to S. S. B.). This work was also supported by the High-Tech Fund of the Dana-Farber Cancer Institute, postdoctoral fellowships from the Spanish Ministerio de Educación y Ciencia (to L. G.), and a National Science Foundation predoctoral fellowship (to P. S. K.). Affymetrix Inc. is a for-profit entity. G. L. V. is a shareholder, consultant to, and corporate officer of Ontorii, Inc., which has secured an option from Harvard University to commercialize the RIPtide technology.
[S] This article contains supplemental Figs. S1 and S2, Table S1, "Experimental Procedures," and additional references.
[1] Present address: Universidad de Alcalá, Carretera N-II, km 33.6, 28871 Alcalá de Henares, Spain.
[2] Present address: Virginia Tech, 3101 Hahn Hall, West Campus Dr., Blacksburg, VA 24061.
[3] Present address: Novartis Institutes for BioMedical Research, 250 Massachusetts Ave., Cambridge, MA 02139.
[4] Present address: Interfacial Solutions, LLC, 949 Antler Ct., River Falls, WI 54022.
[5] To whom correspondence should be addressed: 12 Oxford St., Cambridge, MA 02138. Tel.: 617-495-5323; Fax: 617-495-8755; E-mail: Gregory_verdine@harvard.edu.

Of particular note in the latter regard is the work of Turner and colleagues (15–18), who employed microarrays of 2′-OMe ribonucleotides and locked nucleic acids to perform an independent experimental assessment of the predicted secondary structure for several biologically relevant RNAs. Efforts along these lines to date have involved sparse sampling of ligand sequence space, with at most 320 candidate sequences examined per study, these having been designed on the basis of Watson-Crick complementarity to prospective docking sequences on the RNA target of interest. Microarrays representing all possible ligand sequences would serve the valuable function of providing a more unbiased and comprehensive approach, but these have not been available to date. With the relatively long sequences (>15 nt[6]) of unmodified DNA oligonucleotides typically required to form a stable Watson-Crick pairing with RNA targets, the total number of candidate sequences (4^n, where n equals the number of nucleobases in the oligonucleotide) greatly exceeds the capacity of even the highest density microarrays presently available. The use of nucleoside analogs can boost target affinity, thereby reducing the length of the candidate ligands and hence overall library size, but the use of such analogs requires the development of dedicated methods for fabrication for high density microarrays. Here, we report the development of microarrays that comprehensively represent all sequences of 2′-OMe RNA-interacting polynucleotides (2′-OMe RIPtides) having the four natural nucleobases (A, C, G, and U), and ranging in length from 4- to 8-mers. This screening platform includes a total of 87,296 individual oligonucleotide analog probes, vastly exceeding the few hundreds of nucleic acid binders employed in previously reported microarray studies (13–18).

To illustrate the utility of the 2′-OMe RIPtide microarrays in the unbiased identification of targetable sequences, we chose to target human telomerase, a specialized ribonucleoprotein (RNP) composed of two minimally essential components, a reverse transcriptase protein subunit (hTERT) and an RNA component (hTR) (19, 20), as well as several associated proteins. Telomerase directs the synthesis of telomeric repeats at chromosome ends by using a short sequence within hTR as a template for DNA polymerization via reverse transcription. Telomerase has been found to be up-regulated in ~90% of human tumors, an adaptation believed to arise in order to evade cell cycle arrest through replication-dependent telomere shortening (21, 22). Inhibition of telomerase has thus emerged as an attractive therapeutic intervention for use in the treatment of cancer. Indeed, considerable progress has been made toward developing oligonucleotides that inhibit telomerase by competitively binding the template sequence on hTR used by the enzyme to encode the telomere during extension (23–26). Our goal in this study was to identify additional targetable sites in hTR that might provide structurally and mechanistically distinct alternatives to the template sequence. We chose to screen a structured element of hTR comprising both the template and a pseudoknot element that, like the template, is essential for telomerase function (27, 28). Consistent with this essentiality, and with its high degree of structural conservation across vertebrates (29), mutations in this domain give rise to several telomerase deficiency diseases in humans (30, 31). Several three-dimensional structures of engineered minimal pseudoknot RNAs have been reported (32–34), but the overall structure remains unelucidated. Here, we report the identification of 2′-OMe RIPtides that inhibit telomerase function in biochemical assays and in cultured cells and that may provide starting points for the development of next generation telomerase targeting agents.

EXPERIMENTAL PROCEDURES

Detailed experimental procedures can be found in supplemental material.

Microarray Manufacture—For the fabrication of 2′-OMe oligonucleotide-based high density microarrays, a photoresist technique based in I-line (365 nm) projection lithography was utilized (35). This method (supplemental Fig. S1) differs from that used in the manufacture of Affymetrix GeneChip microarrays, which employs 2′-deoxynucleoside phosphoramidites bearing a photodeprotectable 5′-protecting group. 5′-DMT-2′-OMe phosphoramidites were used as monomers for the on-chip synthesis of the RIPtide microarrays, with a photogenerated acid being used to remove the 5′-DMT group during chain extension. The silica substrate for the arrays was first silanized and then reacted with a hexaethyleneglycol derivative (used as a spacer between the oligonucleotides and the array surface) before the initial nucleic acid coupling step. Then a film containing the photoacid generator was coated onto the substrate, aligned, and exposed in the stepper to the first mask, giving rise to the photogenerated acid for the first detritylation. The film was then removed, and the substrate was processed in a cell flow in which the first DMT-protected phosphoramidite monomer was added. Subsequent steps of capping, oxidation, and washes were carried out, and the process was repeated using the next mask and the next oligonucleotide in the sequence (supplemental Fig. S1). After the synthesis was completed, substrates were treated with a solution of organic base to remove protecting groups from the RIPtides. Wafers were rinsed, spin-dried under nitrogen, and diced into individual chips. The final density of full-length RIPtide on these microarrays was ~30–50 pmol/cm^2, with a feature size of 17.5 μm. The chips also included a checkerboard for grid alignment consisting of the 13-mer 2′-OMe sequence 5′-ACGGTAGCATCTT-3′, which allows hybridization with the commercial Affymetrix Oligo B2 (5′-biotin-GTC-AAGATGCTACCGTTCAG-3′).

RNA Preparation—5′-End Cy3-labeled PKWT and PKWT-1 were purchased from Dharmacon. RNAs fragments of >50 nt were obtained by *in vitro* transcription from a dsDNA template generated by PCR from a pRc/CMV vector containing hTR (Collins laboratory) in the presence of aminoallyl-UTP, as described in the supplemental material. Transcription was performed at 37 °C using T7-RNA polymerase, 4 mM NTPs, 1 unit/ml yeast inorganic pyrophosphatase, RNase inhibitor, and 10× transcription buffer. After DNase I treatment (15–30 min,

[6] The abbreviations used are: nt, nucleotide; RIPtide, RNA-interacting polynucleotide; hTR, human telomerase RNA; RNP, ribonucleoprotein; DMT, 5′-dimethoxytrityl; FAM, 6-carboxyfluorescein; FP, fluorescence polarization; TRAP, telomeric repeat amplification protocol.

37 °C) and purification by denaturing PAGE, the target RNA was labeled with Cy3-NHS ester (Amersham Biosciences, 0.1 M Na_2CO_3, pH 8.5, 50% DMSO/H_2O, 1 h). Excess dye was removed by ethanol precipitation, and the RNA was then purified and desalted.

Microarray Hybridization—A specific probe (Oligo B2, Affymetrix) was first hybridized to the checkerboard to provide a grid alignment guide. Briefly, 250 pM oligonucleotide B2 was hybridized to the RIPtide chip for 16 h at 45 °C and then stained using streptavidin/phycoerythrin. Cy3-labeled RNAs were refolded by heating at 95 °C for 3 min followed by slowly cooling to room temperature in 1× array buffer (50 mM potassium PBS, 150 mM KCl, and 5 mM $Mg(OAc)_2$, pH 7.4). Denaturing polyacrylamide gels (6%) were run as control experiments to check for RNA integrity under the buffer conditions employed for refolding and after 1 h of incubation at 37 °C (supplemental Fig. S2). In addition, RNA samples were also tested after refolding by native gel electrophoresis (6%) to confirm the presence of a major RNA folded population (supplemental Fig. S2). 100 nM folded RNAs were incubated with the RIPtide chips at 37 °C for 1 h. The arrays were washed and scanned using the Affymetrix GeneChip 3000 7G scanner, and microarray images were analyzed using GeneChip Operating Software (Affymetrix Inc.).

Data Analysis and RIPtide Clustering—After raw fluorescence values were averaged, a list of the top 100 hits was extracted (supplemental material) and aligned against the target RNA sequence using Perl scripts developed in-house. The RIPtide sequences were aligned against the target RNA sequence (>60% sequence identity) to identify putative binding sites. The oligonucleotide sequences were aligned at every possible register of the RNA sequence, and the similarity (*S*) was calculated at each register, based on complementarity between the oligonucleotide and RNA sequences (Equation 1),

$$S = \frac{n}{N} \qquad \text{(Eq. 1)}$$

where *n* is the number of complementary bases, and *N* is the length of the RIPtide. This is essentially the Jaccard similarity coefficient, except when the oligonucleotide hangs off the RNA sequence. The RIPtide was allowed to hang off the RNA sequence on the ends, and in these cases, the number of matching bases was divided by the length of the oligonucleotide (not the number of bases that overlap, in contrast to the Jaccard similarity coefficient) to generate a similarity score. Only canonical Watson-Crick base pairing was considered, and commonly occurring wobble pairs, such as the G·U wobble pair (36), were not taken into account. Alignment was achieved at the position with maximum similarity between the oligonucleotide and RNA sequence, and the center of where the oligonucleotides sequence mapped to the RNA sequence was recorded. For example, if the RIPtide oligonucleotide mapped to RNA bases 11–15, 13 was the center. In the cases of RIPtides with an even number of bases, the resulting value for the center was rounded up. The number of oligonucleotides centered on each RNA base was calculated and plotted, as shown in Fig. 3. From these plots, groups of RIPtides emerged, as denoted by peaks spanning ~2–3 adjacent RNA bases. These groups of oligonucleotides were manually clustered based on where major peaks started and stopped. Although this clustering step could have been automated based on the number of RIPtides targeting adjacent bases (*i.e.* in a similar manner to which peaks are identified on a chromatogram plot), it was unnecessary to automate this process because only a handful of clusters was apparent upon visual inspection of where the highest affinity RIPtides (according to microarray experiments) mapped onto the RNA sequence.

Fluorescence Polarization (FP) Assays—FAM-labeled RIPtides were synthesized on a 3′-(6-fluorescein) CPG support (Glen Research) using a MerMade 12 (BioAutomation) DNA synthesizer, purified with Poly Pak-II (Glen Research) cartridges, and compositionally verified by MALDI-TOF MS. Unlabeled full-length hTR was prepared by *in vitro* transcription. After DNase I treatment and ethanol precipitation, hTR was purified using the RNeasy Midi kit (Qiagen). Unlabeled PKWT and PKWT-1 were purchased from Dharmacon. FAM-labeled RIPtides (5 nM) were incubated with increasing concentrations of folded RNA at 37 °C for 2 h, after which FP was recorded at 25 °C using a SpectraMax M5 (Molecular Devices) plate reader. For mapping of hTR-RIPtide-binding sites, full-length hTR transcripts incorporating two consecutive base mutations (to their complementary bases) were generated through site-directed mutagenesis on the pRc/CMV plasmid, using a QuickChange-XL mutagenesis kit (Stratagene), and confirmed by sequencing.

Activity Assays—Telomerase-positive cells were either purchased from ATCC (DU145 and HEK293) or provided in the Chemicon TRAP kit (HeLa). Cell extracts were prepared from cell pellets by detergent lysis with 1× CHAPS buffer (Chemicon). Purified RIPtides were incubated with the extract for 1 h at 37 °C prior to the TRAP assays. Extension of the fluorescent artificial substrate (37) by telomerase was carried out for 30 min at 30 °C, followed by amplification with 30 PCR cycles (34 °C 30 s, 59 °C 30 s, and 72 °C 1 min). The extension products were separated on 10% native polyacrylamide gels, and bands were visualized by fluorescence imaging and quantified using ImageQuant™ (GE Healthcare). Several controls were included in the design of the experiments as follows: a positive control (untreated cell lysate), negative controls (buffer only, heat-inactivated, or RNase-treated cell extracts), and PCR amplification control (60 μM of RIPtide added after telomerase elongation and before PCR step). For cell-based TRAP assays, DU145 cells were transfected with 0.2% Lipofectamine™ 2000 (Invitrogen) and 165 nM RIPtide for a period of 24 h. Cells were harvested, counted, lysed with 1× CHAPS lysis buffer, and normalized by total protein concentration (Bradford assay).

RESULTS

Our goal at the outset was to develop a microarray platform that would enable a structurally unbiased screen to identify RIPtides that bind with high affinity to a folded RNA target (Fig. 1) and ultimately to use the RIPtides thus identified to modulate the activity of the target RNA in cells. As cell permeability of oligonucleotides decreases as a function of length (38, 39), and with the knowledge that backbone modification can confer on short nucleic acid sequences the ability to bind tightly and spe-

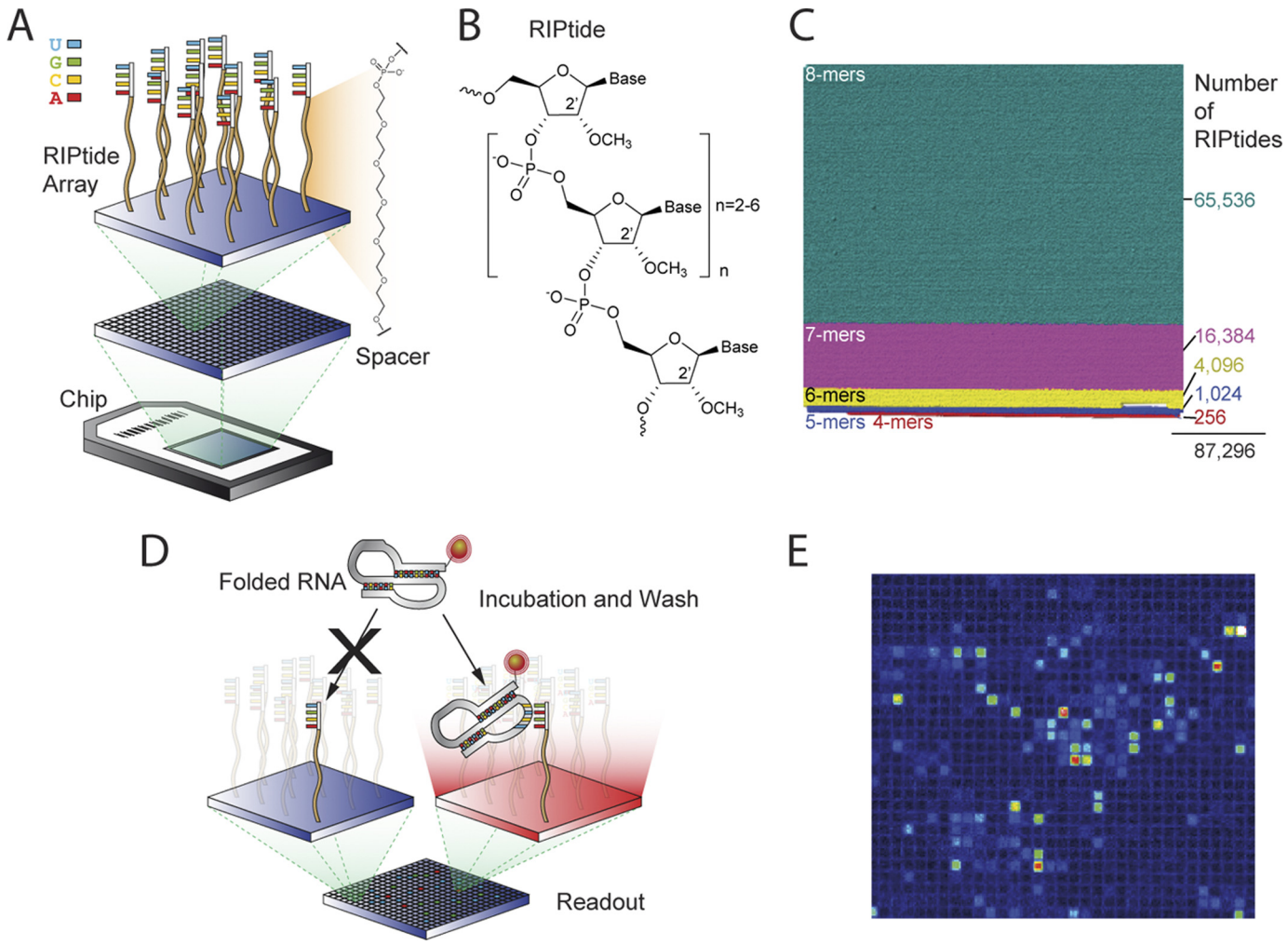

FIGURE 1. **Overview of the RIPtide microarray technology.** *A*, schematic representation of a RIPtide microarray. A PEG linker is used as spacer between the RIPtides and the microarray surface. *B*, chemical structure of the 2′-OMe RIPtides. *C*, RIPtide array format, containing a total 87,296 RIPtide sequences, color-coded according to the number of RIPtides per *N*-mer family. *D*, RIPtide screening protocol. *E*, sample image of an RNA target (PKWT-1) bound to a RIPtide microarray. Hit color scale is displayed as rainbow scale: *red* represents the highest fluorescent intensity and *blue* the lowest. The array fabrication process is summarized in supplemental Fig. 1.

cifically to RNA targets (40, 41), we focused our attention on identifying RIPtides having eight nucleotides or less. In addition, we incorporated 2′-OMe substituents on all of the RIPtides displayed on the microarray (Fig. 1, *A* and *B*), a modification known to increase oligonucleotide affinity for RNA targets (42, 43) as well as stability toward nucleolytic degradation; this modification has previously been used by Turner and co-workers (13–18) to increase the resolution of RNA structure-mapping by microarray screening.

Although 2′-*O*-methylation was expected to provide substantial performance benefits, it also complicated the fabrication of the microarrays, because a direct application of the established Affymetrix platform for photochemically directed high density microarray synthesis (44) would have required the preparation of 5′-photocaged 2′-OMe phosphoramidites. To avoid this laborious operation, we used a recently developed microarray fabrication technology that employs photochemical generation of an acid to deprotect DMT groups (35). This method (supplemental Fig. S1) is particularly well suited to our purpose, because it requires only standard, commercially available 2′-OMe RNA phosphoramidites and can in principle be used with any 5′-DMT-protected nucleic acid analog. It allowed us to generate microarrays displaying on each chip all possible 8-, 7-, 6-, 5-, and 4-mer 2′-OMe RIPtides having the standard nucleobases A, C, G, and U, a total of 87,296 RIPtides (Fig. 1*C*).

Our strategy was to screen the microarray using folded hTR constructs incorporating a fluorescent label, such that the fluorescence intensity of the scanned microarray would read out positive RIPtide "hits" (Fig. 1, *D* and *E*). To investigate the extent to which the size of the RNA target influences its ability to access the RIPtides on the microarray, we constructed a truncation series representing progressively smaller versions of the template/pseudoknot domain, with the smallest being two 48-nt engineered minimal pseudoknots, PKWT and PKWT-1. Cy3-labeled full-length hTR (nt 1–451), PK (nt 1–211), PK175 (nt 26–200), PK159 (nt 33–191), and PK123 (nt 63–185) (Fig. 2*B*) were generated by *in vitro* transcription, whereas the previously reported PKWT construct (32) and PKWT-1 were produced by solid-phase synthesis. PKWT encompasses the hTR sequence between nucleotide positions 93 and 121 and 166 and 184, with an engineered connection between nucleotides 121

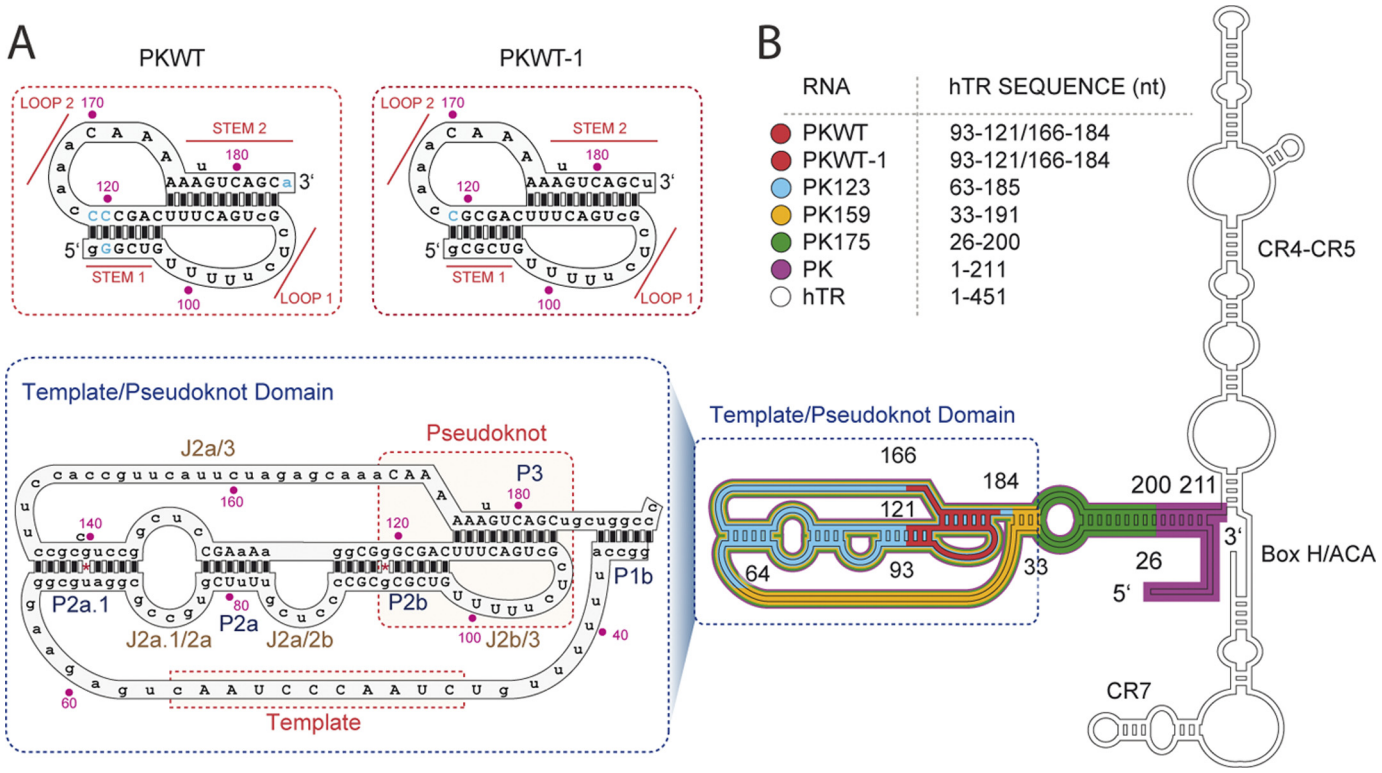

FIGURE 2. **Schematic diagram with the sequences and the predicted secondary structures of the hTR constructs used in this study.** *A*, engineered hTR pseudoknot constructs (PKWT and PKWT-1, *top*) and sequence of the template/pseudoknot domain (*bottom*) of hTR. Bases in *blue font* are non-native sequence. *Capital letters* correspond to residues ≥80% conserved in vertebrates. *B*, secondary structure model of hTR, adapted from Ref. 29, including a schematic representation of the different RNA constructs screened with the RIPtide platform.

and 166 (Fig. 2*A*). PKWT-1 is a variant of PKWT, in which most of the mutations have been restored back to the wild-type sequence.

To encourage folded structure, all hTR constructs were refolded by heating and slowly cooling to ambient temperature in a buffer containing 5 mM magnesium. Under these conditions, all RNA constructs except PKWT showed a major folded population, as evidenced by native gel PAGE experiments (supplemental Fig. S2). Labeled RNAs were incubated with the RIPtide microarrays for varying lengths of time (1, 2, 6, 12, and 18 h), at different temperatures (25 and 37 °C), and at concentrations ranging from 1 to 100 nM. In an initial screen, full-length hTR and the PK construct failed to show quantifiable binding to the microarray; and the slightly shorter PK175 construct gave irreproducible results. However, PK159 and all shorter versions (Fig. 2*B*) yielded reproducible microarray positives. We observed a similar size cutoff in studies of the hepatitis C virus internal ribosome entry site (HCV-IRES).[7] We therefore conclude that the 2′-OMe microarrays reliably provide results with RNA targets shorter than ~160 nt in length but may not yield useful results with RNA targets longer than this.

After optimization of the screening protocol using the PKWT, PKWT-1, PK123, and PK159 constructs, the RIPtide microarrays were incubated with 100 nM RNA target for 1 h at 37 °C, then washed, and scanned. The most intense RIPtide hits were identified by ranking them according to their average raw fluorescence intensity from at least two independent experiments (supplemental material). If, as one might expect, there exist preferred binding sites for the RIPtides on the target RNA, then the hits would be expected to fall into clusters having related sequences and target binding sites. We thus wrote Perl scripts (supplemental material) to assess several different potential modes of clustering the top 100 RIPtide hits. Attempts to cluster the RIPtide hits based solely on their sequence complementarity to one another was found not to produce unambiguously meaningful clusters, because it was difficult with such short sequences to assign a correspondence score to frame-shifted sequences and to sequences having several positions of nonidentity. We therefore clustered the hits using their partial sequence complementarity to the RNA target as a guide. In doing so, we found that RIPtides having nonidentical but overlapping sites of partial complementarity with the target could readily be clustered. Following alignment of the RIPtide hits with the target sequence, we constructed a plot of the sites of partial complementarity on the target against the number of hits for each site (Fig. 3). Only those oligonucleotides having >60% sequence identity to the target RNA were clustered.

In microarray screens using PKWT and PKWT-1 (Fig. 3*A*), all 100 top RIPtide hits could be clustered, and the majority of these belonged to a pair of clusters complementary to two regions of the RNA, either the 5′ terminus of the pseudoknot (part of the P2b stem), designated cluster I, or the J2b/3 loop and an adjacent segment of the P3 stem, designated cluster II. Interestingly, although PKWT differs from PKWT-1 at only three nucleotides, the two RNA targets show a substantial dif-

[7] W. L. Santos and G. L. Verdine, unpublished results.

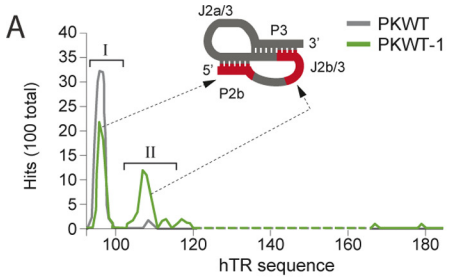

B

Cluster	Sequence (5′-3′)	Microarray Ranking	K_d (PKWT-1, nM)
II	CAGCGAGA	1	43 ± 5
I	GACAGCGC	2	42 ± 6
II	CAGCGAGG	3	n.d.
II	GUCAGCGA	4	30 ± 2
II	ACAGCGAG	5	n.d.
I	AACAGCGC	6	33 ± 9
II	CAGCGAG	7	70 ± 9
II	UCAGCGAG	8	>430
I	ACAGCGCA	9	n.d.
II	AGUCAGCG	10	65 ± 17

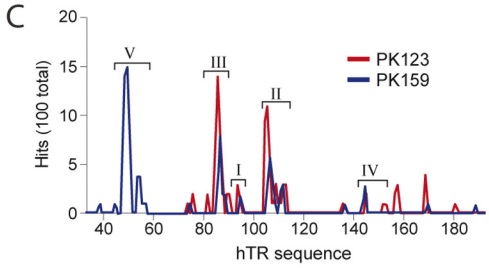

D

Cluster	Consensus sequence	Central position in hTR
II	XAGCGAX	107
III	XGGAGCAX	86
IV	GAAGGCG	145
IV	GAACGGUG	152
V	XGGUUAGX	49
V	AGUUAGG	54

FIGURE 3. **Summary of RIPtide microarray results.** *A*, cluster profiles of PKWT and PKWT-1 (100 nM, 1 h). Number of hits (out of 100) are represented (*y* axis) *versus* nt position from the 5′-end of the screened RNA construct (*x* axis, expressed relative to hTR sequence). *B*, rank of top 10 RIPtide hits and K_d values determined in triplicate with unlabeled PKWT-1. *n.d.*, not determined. *C*, cluster profiles of PK123 and PK159 using standard conditions. *D*, summary of screening results for the hTR/pseudoknot domain, showing the consensus RIPtide sequences for the identified clusters (with *X* representing variable length), and the hTR nt that aligns with the middle (4th) position of the RIPtide. Data represent average ± S.D. of three independent samples.

ference in the relative proportion of hits in cluster I and cluster II, indicating that the microarray can be exquisitely sensitive to such subtle changes of sequence and conformation in the target RNA.

When larger hTR constructs were subjected to the RIPtide screen (Fig. 3*C*), additional regions on the target apparently amenable to binding were identified. For PK123, cluster I hits were considerably diminished, although cluster II remained well represented, but the most prominent cluster of hits now observed was that complementary to the bulge J2a/J2b (nt 82–89), designated cluster III. Several smaller clusters at the 5′-end of the J2a/3 single-stranded region (nt ~142–170, including cluster IV, nt 142–156) were also observed. Finally,

A

RIPtide	hTR-targeted sequence	Region	Sequence (5′-3′)	K_d, hTR (FP, nM)
I-1	93-100	P2b	AACAGCGC	>1,700
I-2	93-99	P2b	ACAGCGC	>2,200
II-1	103-110	J2b/3-P3	CAGCGAGA	34 ± 6
II-2	105-112	J2b/3-P3	GUCAGCGA	3 ± 0.5
II-3	102-109	J2b/3-P3	AGCGAGAA	52 ± 9
III-1	83-88	J2a/2b	GGAGCA	7 ± 1
III-2	81-88	J2a/2b	GGAGCAAA	6 ± 1
IV-1	142-148	P2a1-J2a/3	GAAGGCG	297 ± 98
IV-2	149-156	J2a/3	GAACGGUG	15 ± 3
V-1	46-52	Template	GGGUUAG	4 ± 1
V-2	46-53	Template	AGGGUUAG	4 ± 0.5
V-3	51-57	Template	AGUUAGG	108 ± 17

B

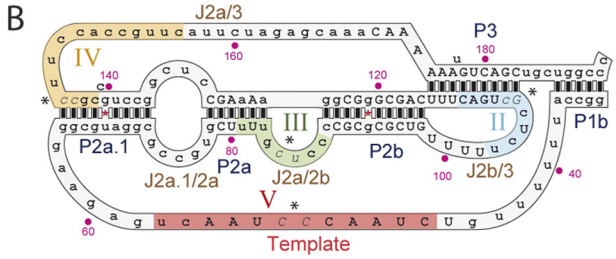

FIGURE 4. **2′-OMe RIPtide mapping of the pseudoknot domain of hTR.** *A*, dissociation constants (nM) for selected RIPtides and unlabeled full-length hTR. Clusters are color-coded. *B*, targetable regions in the template/pseudoknot domain of hTR are colored and indicated on the secondary structure of the hTR core. Bases in *italics* (near an *asterisk*) indicate the mutation sites for FP studies. *Capital letters* are residues ≥80% conserved in vertebrates. Data represent average ± S.D. of triplicates.

for construct PK159, representing the complete template/pseudoknot domain of hTR, a cluster profile similar to that for PK123 was generated, with one major exception as follows: the most prominent cluster observed with PK159 represented RIPtides complementary to the template region (cluster V, nt 47–57), which was absent in all the other constructs.

To assess the ability of the RIPtide hits to bind the target RNA in solution, we selected a panel of RIPtides representing variations on the consensus sequences of top hits for each cluster, and we synthesized them with a FAM label attached to the 3′-end, the same end by which they had been attached to the microarray surface. FP was then used to measure K_d values of the FAM-labeled RIPtides. We first selected a representative sample of the top RIPtide hits from the PKWT-1 screen. As seen in Fig. 3*B*, all but one of these RIPtides bound PKWT-1 with a K_d <100 nM, and we observed a rough correlation between rank order in the microarray screen and affinity for PKWT-1, with RIPtides of lower rank generally having lower affinity for PKWT-1.

It is possible that RIPtide-binding sites present or available in truncated forms of hTR may not be present or available in full-length hTR. We thus selected five RIPtides that had been validated for binding PKWT-1 in solution, and we measured their binding affinity to full-length hTR using FP. As seen in Fig. 4*A*, none of the cluster I hits showed any measurable affinity for hTR, whereas the cluster II hits showed at least as high an affinity for hTR as for PKWT-1. We hypothesize that the cluster I hits became inactive because the end of the pseudoknot to which they bind in PKWT-1 is highly engineered and thus markedly divergent from hTR, whereas the J2b/3 loop to which the cluster II hits bind is retained in full-length hTR. Were the J2b/3 loop involved in tertiary interactions in hTR, RIPtide

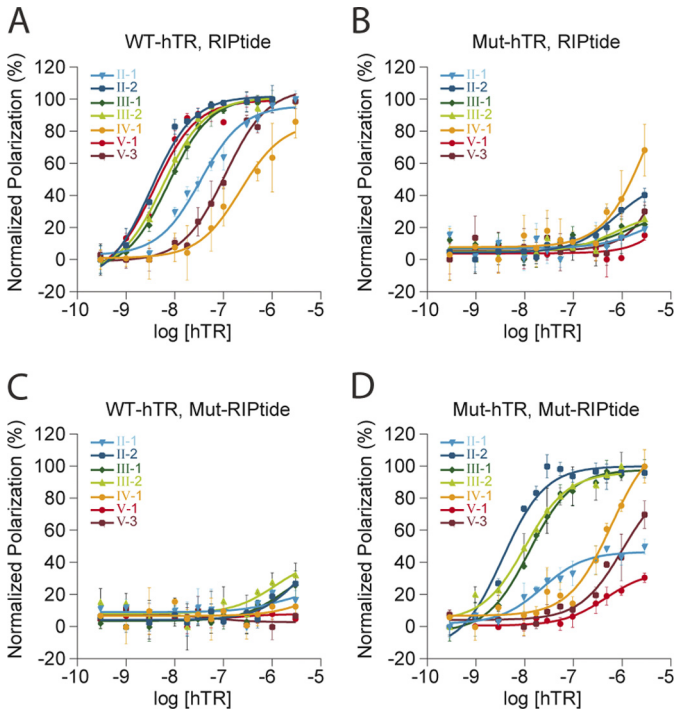

FIGURE 5. **Compensatory mutation studies showing the FP binding curves for hTR-RIPtide interactions.** Assays were performed in triplicate, in the presence of mutated full-length hTRs, mutated RIPtides, or both. 3′-FAM-labeled RIPtides were mutated at the two central bases to their complementary bases. Similarly, four mutant hTRs were generated (mutation sites shown in Fig. 4). Binding profiles are as follows: WT-hTR and RIPtides (*A*); mutant hTR and wild-type RIPtides (*B*); WT-hTR and mutant RIPtides (*C*). *D*, mutant hTR and mutant RIPtides. Polarization in *B–D* was renormalized relative to the WT-hTR, RIPtide situation (*A*).

binding might have been lost, and we therefore surmise that the loop remains relatively unengaged in such interactions when present in naked hTR.

We then went straight to validation of the remainder of the RIPtide hits from PK123 and PK159 microarray screens using full-length hTR. We selected representative RIPtide examples from each of the clusters (Fig. 3*D*), quantified their binding affinity by FP (Fig. 4*A*), and identified RIPtides from clusters III–V that bind full-length hTR. Taken together, the collection of hTR-validated RIPtides maps out a series of sites on the template/pseudoknot especially conducive to targeting by a 2′-OMe polyribonucleotide (Fig. 4*B*, *color-coded*). Specifically, these hyper-targetable regions are the J2b/3 loop and P3 stem (cluster II), the J2a/2b bulge through part of the P2a stem (cluster III), the J2a/3 loop (cluster IV), and the template region (cluster V).

To this point, we had inferred the RIPtide-binding sites on hTR assuming Watson-Crick complementarity between the RIPtide and target. To verify this experimentally, we introduced tandem point mutations into the central portion of the FP-positive RIPtides, along with compensatory sequence changes into hTR. The binding behavior of the "wild-type" and "mutant" RIPtides to wild-type and compensatory mutant hTR targets was analyzed by FP (Fig. 5). Four different hTR transcripts were generated in which two consecutive nucleotides at the central position of each predicted target site (Fig. 5*B*) were mutated to their Watson-Crick complementary bases (G→C, C→G, and U→A). In each case, either by incubating the mutated hTR with the wild-type RIPtide (Fig. 5*B*) or the mutated RIPtides with wild-type hTR (Fig. 5*C*), binding was abolished or severely reduced. When compensatory mutations were introduced into both the RIPtide and hTR (Fig. 5*D*), binding was partially or fully restored in most cases, confirming and supporting the notion that the RIPtides indeed bind hTR at the predicted sites.

Having discovered a panel of RIPtides that bind four different regions on naked hTR, we investigated whether these molecules could inhibit the activity of the telomerase RNP complex *in vitro*. We used the Cy5-TRAP assay (37), a variation of the TRAP (22), to determine IC_{50} values for several RIPtides using HeLa cell extracts. We first tested a library containing 8-, 7-, and 6-mers, fully complementary to the target hTR sequence, with K_d values for hTR <300 nM. We additionally tested several phosphorothioate variations of this initial library (supplemental Table 1). In the first round of experiments, we observed significant inhibition only by 8-mer RIPtides complementary to the template (supplemental Table 1, entries 50 and 55). In addition, we found that several phosphorothioated RIPtides from clusters II–IV inhibited telomerase with IC_{50} values in the micromolar range.

To enhance the potency of certain RIPtides that showed inhibition, we increased their length by 2–3 nt at either end, maintaining Watson-Crick pairing with hTR. Although this strategy did not improve the activity of cluster II or cluster III RIPtides, a significant increase in potency was observed for clusters IV and V RIPtides. Interestingly, we found that several sequence-extended versions of cluster IV RIPtides showed nanomolar IC_{50} values in TRAP assays (supplemental Table 1, entries 35–40). These observations are consistent with previous observations that longer DNA oligonucleotides targeting an overlapping region in hTR exhibit inhibitory activity against telomerase *in vitro* (45).

Next, we performed some limited optimization of RIPtides that target this site starting from a 14-mer covering hTR sequence 143–156 nt, followed by serial truncations on either end, until we identified a minimal sequence comprising 10 nucleotides (complementary to hTR 143–152 nt, supplemental Table 1, entry 32), from which removal of additional bases abolished telomerase inhibition *in vitro*. All RIPtide sequences that included this minimal sequence and possessing a length of 10 nt or longer inhibited telomerase activity with an IC_{50} <10 nM. Thus, through a combination of RIPtide microarray screening and systematic extension guided by TRAP assays, we were able to identify a novel minimal sequence that produces efficient telomerase inhibition *in vitro*. This sequence, 5′-GGUGGAAGGC-3′ (IV-3), inhibited telomerase activity in all cell lines tested (HeLa, DU145, and HEK293), with IC_{50} values in the low nanomolar range (Fig. 6*A*). Moreover, phosphorothioate substitution provided RIPtides that retained their ability to inhibit telomerase very efficiently (Fig. 6*A*, RIPtides IV-4 and IV-5), with IC_{50} values in good agreement with the K_d values determined by FP experiments (Fig. 6, *A–C*). In all cases, mismatch-containing RIPtides were used as negative controls to rule out nonsequence-specific effects (Fig. 6 *legend*) (46).

A

RIPtide	Sequence (5′-3′)	Backbone, Sugar	IC_{50} (TRAP) HeLa	DU145	HEK293T	K_d (FP, nM)
IV-3	GGUGGAAGGC	PD, 2′-OMe	7 ± 2	3.6 ± 0.4	4	4.2 ± 1.5
IV-4	gGUGGAAGgC	PD/PS, 2′-OMe	27 ± 12	12 ± 2.5	n.d.	4.6 ± 0.8
IV-5	gguggaaggc	PS, 2′-OMe	7 ± 0.5	9 ± 1.5	9	8.6 ± 3.4

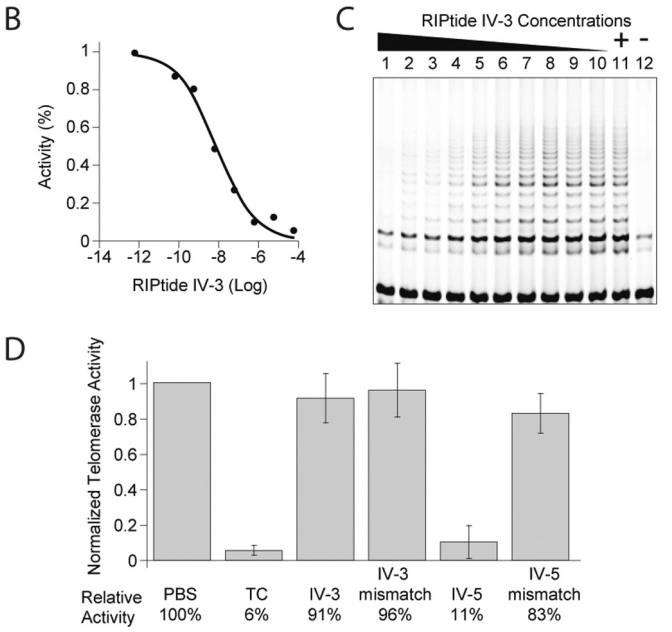

FIGURE 6. **Summary of telomerase inhibition experiments.** *A*, cluster IV RIPtides with anti-telomerase activity. *PD,* phosphodiester; *PS,* phosphorothioate. *Lowercase font* indicates a phosphorothioate linkage. IC_{50} and K_d values are reported in nM. Mismatches in control RIPtides are underlined: GGUGCAAGGC, GGUGCCAGGC (mismatch IV-3), GCUGCAACGC, and ggugccaggc (mismatch IV-5). PCR inhibition control, 60 μM RIPtide. *n.d.* = not determined. *B*, dose-response inhibition by RIPtide IV-3. *C*, TRAP gel showing telomerase inhibition by RIPtide IV-3 in HeLa extracts. *Lane 1,* 60 μM; *lane 2,* 6 μM; *lane 3,* 600 nM; *lane 4,* 60 nM; *lane 5,* 6 nM; *lane 6,* 600 pM; *lane 7,* 60 pM; *lane 8,* 6 pM; *lane 9,* 0.6 pM; *lane 10,* 0.06 pM; *lane 11,* positive control (untreated cell lysate); *lane 12,* negative control (buffer). *D*, *bar graph* showing inhibition by RIPtides IV-3 and IV-5 in DU145 cells, after treatment with 165 nM of RIPtide for 24 h. Lipofectamine™ 2000 was used as transfecting agent. Telomerase activity was normalized relative to a mock transfection (no RIPtide). *TC* is a 13-mer 2′-OMe oligonucleotide complementary to the hTR template (positive control) (23). *Error bars* in *D* are S.D. of triplicates, and experiments were performed at least twice with similar results.

Finally, we tested phosphodiester and phosphorothioate RIPtides IV-3 and IV-5 for intracellular stability in cell-based assays, using a method similar to one previously reported for intracellular use of template-directed oligonucleotides (24). DU145 prostate cancer cells were treated with 165 nM RIPtide for 24 h and subsequently lysed, and their telomerase activity was assessed by TRAP (Fig. 6*D*). As a positive control, a 13-mer 2′-OMe oligonucleotide with terminal phosphorothioate linkages targeting the hTR template was used (23). Lipofectamine™ was added to ensure delivery; it remains to be established whether this is necessary for 10-mers, as relatively short phosphorothioates targeting telomerase have shown optimal cellular uptake (39). Although cells treated with RIPtide IV-3 showed no significant inhibition, RIPtide IV-5 did produce marked inhibition of telomerase, possibly reflecting the greater stability of the latter. Importantly, introduction of two point mutations into RIPtide IV-5, known to abolish telomerase inhibition in extract-based experiments, also abolished inhibition in these cell-based experiments, supporting a mechanism of inhibition in these cell-based assays that, as in pre-lysed extracts, is sequence-specific. To our knowledge, no oligonucleotide targeting this region has previously been shown to inhibit telomerase activity in cultured cells, and we believe that these assays are the first step in assessing RIPtide IV-5's potential as a candidate for cancer cell proliferation studies.

DISCUSSION

Here, we have described a new microarray-based platform for the sequence-unbiased discovery of short polynucleotides that target folded RNA molecules. The key component of this platform is an *N*-mer microarray presenting all possible sequences of 2′-OMe RNA having between 4 and 8 nucleotides in length ($n = 4–8$) and bearing the four canonical RNA bases (A, C, G, and U). To our knowledge, this study describes the first example of a microarray bearing all possible sequences of a nucleic acid analog oligomer. The microarrays reported here possess greater than 87,000 individual RIPtides spatially arrayed, a number several orders of magnitude larger than the few hundreds of nucleic acid binders employed in previously reported microarray studies. The virtue of such large RIPtide arrays is that they enable sequence-unbiased, comprehensive screening of all possible RIPtides up to a given size (8-mer in this study), and as such are expected to provide a more detailed and exhaustive probing of accessible sites in a target RNA. Although the studies reported here were performed under conditions that had been optimized for equilibrium binding of RIPtides to their RNA targets, we have seen in preliminary studies that the 2′-OMe RIPtide microarrays can also provide information on the kinetics of target interaction.[8] The construction of these high density arrays of a nucleic acid analog was made possible by a key advance in microarray synthesis technology, namely photoresist-based deprotection, which has the attractive feature of being compatible with commercially available 5′-DMT-protected 3′-phosphoramidites. This same technology should be directly applicable to the fabrication of RIPtide microarrays bearing other varieties of potentially interesting and useful nucleic acid analogs, such as locked nucleic acids (47), 2′-methoxyethyl-substituted RNAs (48), and glycidyl nucleic acids (49), to name just a few.

At least in principle, another advantage of a sequence-unbiased microarray screen is that it could capture sequences that bind via noncanonical modes of binding, which are known to be an important element of the interaction landscape for RNA. In the present screens, however, we found no clear example of a high affinity noncanonical binder. It is possible that a more exhaustive analysis of a much greater number of hits would yield such noncanonical binders. It is equally possible that noncanonical binding is disfavored with the relatively short sequences employed here, or that such binding modes require stabilizing interactions provided by the 2′-OH group, and that the 2′-OMe is less effective at engaging in these kinds of interactions. Indeed, high resolution structures of structures of RNA have revealed extensive involvement of the 2-OH group in a wide

[8] L. Gude and G. L. Verdine, unpublished results.

variety of noncanonical association modes (50). In the future, we aim to test this hypothesis by fabricating microarrays having a 2′-OH or a functional equivalent. It would also be of great interest to expand the alphabet of nucleobases represented in RIPtide arrays to include those with substantial propensity to pair in Hoogsteen or other modes, such as 8-oxo- and 8-amino derivatives of guanine and adenine.

The RIPtide screening experiments reported here have identified four regions on the telomerase pseudoknot/template region that are available for binding short 2′-OMe polynucleotides. Of these regions, the one that bound the largest number of RIPtides (cluster V) is the template. This is not surprising, as the template region is well known to be targetable by exogenous nucleic acid ligands, and this fact jives well with the biological function of the template as a sequence available for pairing with its nucleic acid substrate, the telomere. Furthermore, that the template engages microarray-bound RIPtides provides validation for the method as a screen for especially productive binding sites in a folded RNA target. The observation that so few sites on the RNA turn out to be targetable by RIPtides and that all the sites identified in the present screens are known from structural probing and sequence covariation to have at least partial single-stranded character (29, 51, 52) provide further evidence that the RNA target adopts a folded structure related to that depicted in folding diagrams. That said, certain regions in the pseudoknot/template that might be predicted on the basis of secondary structure alone to be accessible turn out not to be productive for RIPtide binding, such as the J2a.1/2a bubble, the 5′- and 3′-ends of the template, and the entire 3′-end of the J2a/3 loop (Fig. 3*C*). High resolution structures of folded RNA molecules have revealed that regions suggested by folding diagrams to be single-stranded are often in fact paired, frequently via noncanonical interactions. We note that although the regions targeted by RIPtides from clusters II–IV are partially single-stranded, in each case the targeted region extends into an adjacent segment believed to form a Watson-Crick duplex, and in several instances the cluster preferentially migrates into the adjacent duplex in preference to engaging an adjacent segment of the same loop. This observation is consistent with previously reported data on the strand invasion phenomenon produced by short oligonucleotides binding to RNA (7–9). In addition, the 2′-OMe RIPtide microarrays have revealed a strong propensity of the oligonucleotides to invade at the ends of duplex regions. Similar conclusions can be drawn from previously reported data by Turner and co-workers (17, 18) using isoenergetic microarrays.

The approach followed here, RIPtide microarray screening of isolated RNA elements from a large ribonucleoprotein particle, could stand improvement in certain important respects. One of the most significant issues is that the microarrays lose their binding capacity with RNAs greater than 160–175 nt in length, which is most likely caused by size-sieving on the surface of the microarray. We believe that this limitation can be overcome in the future through the incorporation of a long hydrophilic spacer such as poly(ethylene glycol) between the RIPtide and the microarray surface. Fortunately, many folded, functional RNA elements, including miRNAs and their precursors, are below the present size limit of RIPtide microarrays; but with larger RNAs such as hTR, a domain-based approach must be employed, with all the attendant caveats. In the case of telomerase, there is the further complication that the active form of the enzyme is a protein-RNA assembly and that targetable sites on the RNA alone may not be accessible in the RNP enzyme. This is not necessarily disadvantageous in the present case, as blockade of telomerase assembly is a valid means of inhibiting enzyme function (53, 54). Telomerase RNP assembly is a complex, multistep process (55, 56), one that is not entirely understood, and future studies will be required to determine whether the inhibitors described here operate via inhibition of the telomerase RNA, by interference with assembly, or by some other mechanism. Notwithstanding the aforementioned limitations, via the domain-based RIPtide screening strategy followed by efficacy optimization, we succeeded in identifying a novel 10-mer that inhibits human telomerase activity *in vitro* and in cultured cells. Studies to further test the biological and pharmacologic properties of this molecule as a telomerase antagonist are ongoing.

Acknowledgments—Affymetrix Inc. generously supported all aspects of the microarray fabrication. We thank Prof. Kathleen Collins (University of California at Berkeley) for providing the hTR plasmid and Jennifer Couget (FAS Center for Systems Biology, Harvard), for help with microarray instrumentation. We also thank Eric D. Smith for invaluable assistance with figure preparation and Verdine laboratory members for critical reading of the manuscript.

REFERENCES

1. Hopkins, A. L., and Groom, C. R. (2002) The druggable genome. *Nat. Rev. Drug Discov.* **1,** 727–730
2. Lagoja, I. M., and Herdewijn, P. (2007) Use of RNA in drug design. *Expert Opin. Drug Discov.* **2,** 889–903
3. Thomas, J. R., and Hergenrother, P. J. (2008) Targeting RNA with small molecules. *Chem. Rev.* **108,** 1171–1224
4. Hermann, T. (2007) Aminoglycoside antibiotics. Old drugs and new therapeutic approaches. *Cell. Mol. Life Sci.* **64,** 1841–1852
5. Welch, E. M., Barton, E. R., Zhuo, J., Tomizawa, Y., Friesen, W. J., Trifillis, P., Paushkin, S., Patel, M., Trotta, C. R., Hwang, S., Wilde, R. G., Karp, G., Takasugi, J., Chen, G., Jones, S., Ren, H., Moon, Y. C., Corson, D., Turpoff, A. A., Campbell, J. A., Conn, M. M., Khan, A., Almstead, N. G., Hedrick, J., Mollin, A., Risher, N., Weetall, M., Yeh, S., Branstrom, A. A., Colacino, J. M., Babiak, J., Ju, W. D., Hirawat, S., Northcutt, V. J., Miller, L. L., Spatrick, P., He, F., Kawana, M., Feng, H., Jacobson, A., Peltz, S. W., and Sweeney, H. L. (2007) PTC124 targets genetic disorders caused by nonsense mutations. *Nature* **447,** 87–91
6. Hendrix, D. K., Brenner, S. E., and Holbrook, S. R. (2005) RNA structural motifs. Building blocks of a modular biomolecule. *Q. Rev. Biophys.* **38,** 221–243
7. Southern, E. M., Case-Green, S. C., Elder, J. K., Johnson, M., Mir, K. U., Wang, L., and Williams, J. C. (1994) Arrays of complementary oligonucleotides for analysing the hybridization behavior of nucleic acids. *Nucleic Acids Res.* **22,** 1368–1373
8. Milner, N., Mir, K. U., and Southern, E. M. (1997) Selecting effective antisense reagents on combinatorial oligonucleotide arrays. *Nat. Biotechnol.* **15,** 537–541
9. Mir, K. U., and Southern, E. M. (1999) Determining the influence of structure on hybridization using oligonucleotide arrays. *Nat. Biotechnol.* **17,** 788–792
10. Sohail, M., Akhtar, S., and Southern, E. M. (1999) The folding of large RNAs studied by hybridization to arrays of complementary oligonucleotides. *RNA* **5,** 646–655

11. Sohail, M., Hochegger, H., Klotzbücher, A., Guellec, R. L., Hunt, T., and Southern, E. M. (2001) Antisense oligonucleotides selected by hybridization to scanning arrays are effective reagents *in vivo*. *Nucleic Acids Res.* **29,** 2041–2051
12. Ooms, M., Verhoef, K., Southern, E., Huthoff, H., and Berkhout, B. (2004) Probing alternative foldings of the HIV-1 leader RNA by antisense oligonucleotide scanning arrays. *Nucleic Acids Res.* **32,** 819–827
13. Kierzek, E., Kierzek, R., Turner, D. H., and Catrina, I. E. (2006) Facilitating RNA structure prediction with microarrays. *Biochemistry* **45,** 581–593
14. Duan, S., Mathews, D. H., and Turner, D. H. (2006) Interpreting oligonucleotide microarray data to determine RNA secondary structure. Application to the 3′-end of *Bombyx mori* R2 RNA. *Biochemistry* **45,** 9819–9832
15. Kierzek, E., Kierzek, R., Moss, W. N., Christensen, S. M., Eickbush, T. H., and Turner, D. H. (2008) Isoenergetic penta- and hexanucleotide microarray probing and chemical mapping provide a secondary structure model for an RNA element orchestrating R2 retrotransposon protein function. *Nucleic Acids Res.* **36,** 1770–1782
16. Kierzek, E., Christensen, S. M., Eickbush, T. H., Kierzek, R., Turner, D. H., and Moss, W. N. (2009) Secondary structures for 5′ regions of R2 retrotransposon RNAs reveal a novel conserved pseudoknot and regions that evolve under different constraints. *J. Mol. Biol.* **390,** 428–442
17. Kierzek, E. (2009) Binding of short oligonucleotides to RNA: studies of the binding of common RNA structural motifs to isoenergetic microarrays. *Biochemistry* **48,** 11344–11356
18. Liang, R., Kierzek, E., Kierzek, R., and Turner, D. H. (2010) Comparisons between chemical mapping and binding to isoenergetic oligonucleotide microarrays reveal unexpected patterns of binding to the *Bacillus subtilis* RNase P RNA specificity domain. *Biochemistry* **49,** 8155–8168
19. Nakamura, T. M., Morin, G. B., Chapman, K. B., Weinrich, S. L., Andrews, W. H., Lingner, J., Harley, C. B., and Cech, T. R. (1997) Telomerase catalytic subunit homologs from fission yeast and human. *Science* **277,** 955–959
20. Feng, J., Funk, W. D., Wang, S. S., Weinrich, S. L., Avilion, A. A., Chiu, C. P., Adams, R. R., Chang, E., Allsopp, R. C., and Yu, J. (1995) The RNA component of human telomerase. *Science* **269,** 1236–1241
21. Shay, J. W., and Bacchetti, S. (1997) A survey of telomerase activity in human cancer. *Eur. J. Cancer* **33,** 787–791
22. Kim, N. W., Piatyszek, M. A., Prowse, K. R., Harley, C. B., West, M. D., Ho, P. L., Coviello, G. M., Wright, W. E., Weinrich, S. L., and Shay, J. W. (1994) Specific association of human telomerase activity with immortal cells and cancer. *Science* **266,** 2011–2015
23. Pitts, A. E., and Corey, D. R. (1998) Inhibition of human telomerase by 2′-*O*-methyl-RNA. *Proc. Natl. Acad. Sci. U.S.A.* **95,** 11549–11554
24. Herbert, B., Pitts, A. E., Baker, S. I., Hamilton, S. E., Wright, W. E., Shay, J. W., and Corey, D. R. (1999) Inhibition of human telomerase in immortal human cells leads to progressive telomere shortening and cell death. *Proc. Natl. Acad. Sci. U.S.A.* **96,** 14276–14281
25. Hochreiter, A. E., Xiao, H., Goldblatt, E. M., Gryaznov, S. M., Miller, K. D., Badve, S., Sledge, G. W., and Herbert, B. (2006) Telomerase template antagonist GRN163L disrupts telomere maintenance, tumor growth, and metastasis of breast cancer. *Clin. Cancer Res.* **12,** 3184–3192
26. Dikmen, Z. G., Gellert, G. C., Jackson, S., Gryaznov, S., Tressler, R., Dogan, P., Wright, W. E., and Shay, J. W. (2005) *In vivo* inhibition of lung cancer by GRN163L. A novel human telomerase inhibitor. *Cancer Res.* **65,** 7866–7873
27. Mitchell, J. R., and Collins, K. (2000) Human telomerase activation requires two independent interactions between telomerase RNA and telomerase reverse transcriptase. *Mol. Cell* **6,** 361–371
28. Lin, J., Ly, H., Hussain, A., Abraham, M., Pearl, S., Tzfati, Y., Parslow, T. G., and Blackburn, E. H. (2004) A universal telomerase RNA core structure includes structured motifs required for binding the telomerase reverse transcriptase protein. *Proc. Natl. Acad. Sci. U.S.A.* **101,** 14713–14718
29. Chen, J. L., Blasco, M. A., and Greider, C. W. (2000) Secondary structure of vertebrate telomerase RNA. *Cell* **100,** 503–514
30. Vulliamy, T., Marrone, A., Goldman, F., Dearlove, A., Bessler, M., Mason, P. J., and Dokal, I. (2001) The RNA component of telomerase is mutated in autosomal dominant dyskeratosis congenita. *Nature* **413,** 432–435
31. Vulliamy, T., Marrone, A., Dokal, I., and Mason, P. J. (2002) Association between aplastic anaemia and mutations in telomerase RNA. *Lancet* **359,** 2168–2170
32. Theimer, C. A., Blois, C. A., and Feigon, J. (2005) Structure of the human telomerase RNA pseudoknot reveals conserved tertiary interactions essential for function. *Mol. Cell* **17,** 671–682
33. Kim, N. K., Zhang, Q., Zhou, J., Theimer, C. A., Peterson, R. D., and Feigon, J. (2008) Solution structure and dynamics of the wild-type pseudoknot of human telomerase RNA. *J. Mol. Biol.* **384,** 1249–1261
34. Zhang, Q., Kim, N. K., Peterson, R. D., Wang, Z., and Feigon, J. (2010) Structurally conserved five nucleotide bulge determines the overall topology of the core domain of human telomerase RNA. *Proc. Natl. Acad. Sci. U.S.A.* **107,** 18761–18768
35. Pawloski, A. R., McGall, G., Kuimelis, R. G., Barone, D., Cuppoletti, A., Ciccolella, P., Spence, E., Afroz, F., Bury, P., Chen, C., Chen, C., Pao, D., Le, M., McGee, B., Harkins, E., Savage, M., Narasimhan, S., Goldberg, M., Rava, R., and Fodor, S. P. (2007) Photolithographic synthesis of high density DNA probe arrays. Challenges and opportunities. *J. Vac. Sci. Technol. B* **25,** 2537–2546
36. Varani, G., and McClain, W. H. (2000) The G·U wobble base pair. A fundamental building block of RNA structure crucial to RNA function in diverse biological systems. *EMBO Rep.* **1,** 18–23
37. Herbert, B. S., Hochreiter, A. E., Wright, W. E., and Shay, J. W. (2006) Nonradioactive detection of telomerase activity using the telomeric repeat amplification protocol. *Nat. Protoc.* **1,** 1583–1590
38. Loke, S. L., Stein, C. A., Zhang, X. H., Mori, K., Nakanishi, M., Subasinghe, C., Cohen, J. S., and Neckers, L. M. (1989) Characterization of oligonucleotide transport into living cells. *Proc. Natl. Acad. Sci. U.S.A.* **86,** 3474–3478
39. Chen, Z., Monia, B. P., and Corey, D. R. (2002) Telomerase inhibition, telomere shortening, and decreased cell proliferation by cell permeable 2′-*O*-methoxyethyl oligonucleotides. *J. Med. Chem.* **45,** 5423–5425
40. Childs, J. L., Disney, M. D., and Turner, D. H. (2002) Oligonucleotide-directed misfolding of RNA inhibits *Candida albicans* group I intron splicing. *Proc. Natl. Acad. Sci. U.S.A.* **99,** 11091–11096
41. Childs, J. L., Poole, A. W., and Turner, D. H. (2003) Inhibition of *Escherichia coli* RNase P by oligonucleotide directed misfolding of RNA. *RNA* **9,** 1437–1445
42. Freier, S. M., and Altmann, K. (1997) The ups and downs of nucleic acid duplex stability. Structure-stability studies on chemically modified DNA: RNA duplexes. *Nucleic Acids Res.* **25,** 4429–4443
43. Majlessi, M., Nelson, N. C., and Becker, M. M. (1998) Advantages of 2′-*O*-methyl oligoribonucleotide probes for detecting RNA targets. *Nucleic Acids Res.* **26,** 2224–2229
44. Dalma-Weiszhausz, D. D., Warrington, J., Tanimoto, E. Y., and Miyada, C. G. (2006) The affymetrix GeneChip platform. An overview. *Methods Enzymol.* **410,** 3–28
45. Pruzan, R., Pongracz, K., Gietzen, K., Wallweber, G., and Gryaznov, S. (2002) Allosteric inhibitors of telomerase. Oligonucleotide N3′→P5′ phosphoramidates. *Nucleic Acids Res.* **30,** 559–568
46. Matthes, E., and Lehmann, C. (1999) Telomerase protein rather than its RNA is the target of phosphorothioate-modified oligonucleotides. *Nucleic Acids Res.* **27,** 1152–1158
47. Kaur, H., Babu, B. R., and Maiti, S. (2007) Perspectives on chemistry and therapeutic applications of locked nucleic acid (LNA). *Chem. Rev.* **107,** 4672–4697
48. Bennett, C. F. (2008) in *Antisense Drug Technology: Principles, Strategies, and Applications* (Crooke, S. T., ed) 2nd Ed., pp. 273–303, CRC Press, Inc., Boca Raton, FL
49. Schlegel, M. K., Peritz, A. E., Kittigowittana, K., Zhang, L., and Meggers, E. (2007) Duplex formation of the simplified nucleic acid GNA. *ChemBioChem* **8,** 927–932
50. Leontis, N. B., and Westhof, E. (2001) Geometric nomenclature and classification of RNA base pairs. *RNA* **7,** 499–512
51. Antal M., Boros E., Solymosy, F., and Kiss T. (2002) Analysis of the structure of human telomerase RNA *in vivo*. *Nucleic Acids Res.* **30,** 912–920
52. Gavory, G., Symmons, M. F., Krishnan Ghosh, Y., Klenerman, D., and

Balasubramanian, S. (2006) Structural analysis of the catalytic core of human telomerase RNA by FRET and molecular modeling. *Biochemistry* **45,** 13304–13311
53. Hamilton, S. E., Simmons, C. G., Kathiriya, I. S., and Corey, D. R. (1999) Cellular delivery of peptide nucleic acids and inhibition of human telomerase. *Chem. Biol.* **6,** 343–351
54. Keppler, B. R., and Jarstfer, M. B. (2004) Inhibition of telomerase activity by preventing proper assemblage. *Biochemistry* **43,** 334–343
55. Darzacq, X., Kittur, N., Roy, S., Shav-Tal, Y., Singer, R. H., and Meier, U. T. (2006) Stepwise RNP assembly at the site of H/ACA RNA transcription in human cells. *J. Cell Biol.* **173,** 207–218
56. Stone, M. D., Mihalusova, M., O'connor, C. M., Prathapam, R., Collins, K., and Zhuang, X. (2007) Stepwise protein-mediated RNA folding directs assembly of telomerase ribonucleoprotein. *Nature* **446,** 458–461